Icarus 206 (2010) 594–607

Contents lists available at ScienceDirect

Icarus

journal homepage: www.elsevier.com/locate/icarus

Subsurface heat transfer on Enceladus: Conditions under which melting occurs

Andrew P. Ingersoll [a,*], Alexey A. Pankine [b]

[a] California Institute of Technology, MS 150-21, Pasadena, CA 91125, USA
[b] Jet Propulsion Laboratory/Caltech, MS 183-301, Pasadena, CA 91109, USA

ARTICLE INFO

Article history:
Received 10 December 2008
Revised 3 June 2009
Accepted 19 September 2009
Available online 29 September 2009

Keywords:
Enceladus
Ices
Geological processes
Interiors

ABSTRACT

Given the heat that is reaching the surface from the interior of Enceladus, we ask whether liquid water is likely and at what depth it might occur. The heat may be carried by thermal conduction through the solid ice, by the vapor as it diffuses through a porous matrix, or by the vapor flowing upward through open cracks. The vapor carries latent heat, which it acquires when ice or liquid evaporates. As the vapor nears the surface it may condense onto the cold ice, or it may exit the vent without condensing, carrying its latent heat with it. The ice at the surface loses its heat by infrared radiation. An important physical principle, which has been overlooked so far, is that the partial pressure of the vapor in the pores and in the open cracks is nearly equal to the saturation vapor pressure of the ice around it. This severely limits the ability of ice to deliver the observed heat to the surface without melting at depth. Another principle is that viscosity limits the speed of the flow, both the diffusive flow in the matrix and the hydrodynamic flow in open cracks. We present hydrodynamic models that take these effects into account. We find that there is no simple answer to the question of whether the ice melts or not. Vapor diffusion in a porous matrix can deliver the heat to the surface without melting if the particle size is greater than ~1 cm and the porosity is greater than ~0.1, in other words, if the matrix is a rubble pile. Whether such an open matrix can exist under its own hydrostatic load is unclear. Flow in open cracks can deliver the heat without melting if the width of the crack is greater than ~10 cm, but the heat source must be in contact with the crack. Frictional heating on the walls due to tidal stresses is one such possibility. The lifetime of the crack is a puzzle, since condensation on the walls in the upper few meters could seal the crack off in a year, and it takes many years for the heat source to warm the walls if the crack extends down to km depths. The 10:1 ratio of radiated heat to latent heat carried with the vapor is another puzzle. The models tend to give a lower ratio. The resolution might be that each tiger stripe has multiple cracks that share the heat, which tends to lower the ratio. The main conclusion is that melting depends on the size of the pores and the width of the cracks, and these are unknown at present.

1. Introduction

Whether liquid water is present or not below the surface of Enceladus depends on the efficiency of subsurface heat transfer. Spencer et al. (2006) point out that thermal conduction through solid ice requires a steep temperature gradient, implying melting within 40 m of the surface for a heat flux equal to that of a 124 K blackbody. Recent estimates suggest localized places on the surface with temperatures as high as 223 K (Abramov and Spencer, 2009), implying melting within a few meters of the surface if thermal conduction in the vertical were the only mode of heat transfer. However, heat transfer by latent heat of vaporization is potentially a much more efficient process than thermal conduction, as pointed out by Spencer et al. (2006) and Nimmo et al. (2007), and could carry heat to the surface from sources many km deep without melting.

The term "tiger stripes" is used to identify the four prominent fissures that are seen in images of the South Polar Region (Porco et al., 2006). They are the sources of the most intense infrared radiation (Spencer et al., 2006; Abramov and Spencer, 2009) and most of the plume activity (Spitale and Porco, 2007). The gases in the plumes are mostly water vapor (Hansen et al., 2006, 2008), although other gases make up almost 10% of the mixture (Waite et al., 2006).

Our goal is to use the plume data and data on the surface heat fluxes to estimate subsurface temperatures and decide under what conditions melting occurs. We include heat transfer by the vapor and heat transfer by thermal conduction through the ice. Vapor transfer occurs in two ways. The first is vapor diffusion through pores in an icy matrix. The second is hydrodynamic flow of vapor through open cracks. In both cases, the water molecules pick up

* Corresponding author. Address: Division of Geological and Planetary Sciences, MS 150-21, California Institute of Technology, 1200 East California Boulevard, Pasadena, CA 91125, USA. Fax: +1 626 585 1917.
E-mail address: api@gps.caltech.edu (A.P. Ingersoll).

0019-1035/$ - see front matter © 2009 Elsevier Inc. All rights reserved.
doi:10.1016/j.icarus.2009.09.015

latent heat when they evaporate from the source region, which is assumed to lie below the surface. The molecules diffuse upward or flow upward until they approach the surface. They then either escape as vapor, carrying their latent heat with them, or they condense close to the surface and transfer their latent heat to the ice. The heat is then conducted over a short distance through the ice and radiated to space.

An important principle, which has been overlooked until now, is that the partial pressure of the vapor is nearly the same as the saturation vapor pressure (SVP) of the ice. Nimmo et al. (2007) looked at shear heating driven by tidal stresses in an icy shell that floats on a subsurface ocean. They assumed that 90% of the heating is carried to the surface as vapor, but they ignored the rapid equilibration that takes place between ice and vapor. Their model has vapor densities that are 1000 times greater than saturated vapor at 273 K (Fig. D of the Supplementary Information of their paper). With these high vapor densities, their model overestimates the ability of the vapor to transport heat and therefore underestimates the subsurface temperatures. We argue that melting at shallow depths is more likely than one would infer from their paper.

Gioia et al. (2007) postulate that heat is carried to the surface by "advecting gases," principally water vapor, in a network of "cracked material," which is either water ice or clathrate hydrate. The network from each tiger stripe extends down through 35 km of crust, widens with depth, and finally merges with other networks at the base where the underlying heat source lies. Gioia et al. argue that the ice is cold, and they use the term "Frigid Faithful" to describe their model. We argue that the vapor pressure of cold ice is so low that the advecting gases cannot carry the observed heat flux. This implies that the ice is warm, but then the viscosity of the ice is low. Low-viscosity ice flows in response to hydrostatic pressure, and it is possible that the cracks close up. The time scale depends on the viscosity, which is uncertain by two orders of magnitude, but it could be in the range 1–100 years. If the cracks close up, there is no way to get the heat out without melting.

Abramov and Spencer (2009) assume that condensation of vapor maintains the walls of the crack at a relatively warm temperature, which is independent of depth, and they solve for the heat that is transferred from the walls into the ice and ultimately radiated to space. The wall temperature is a free parameter in their model. They do not model the flow in the crack or the mechanism that would maintain the crack at a particular temperature. Here we assess their assumptions with a hydrodynamic model of flow in an open crack.

Schmidt et al. (2008) focus on particle production in a hydrodynamic flow, but they ignore evaporation and condensation at the walls, which in their model are thermodynamically decoupled from the vapor. They also ignore the viscous interaction between the walls and the fluid. Based on observed particle sizes and speeds, they argue that the source of the flow is at or above the melting point. However, formation of particles depends on the thermodynamic state of the gas, which is strongly affected by interaction with the walls. We argue that positive and negative inferences of melting are premature until the walls are properly treated.

In Section 2 we show that the equilibration of pressures between gas and the wall is almost instantaneous and that the partial pressure of the vapor is close to the SVP of the walls. In Section 3 we show that heat transfer by vapor diffusion through porous ice increases rapidly with increasing temperature, pore size, and grain size. In Section 4 we apply these ideas to Enceladus and show that melting is likely within a few km of the surface unless the ice grain diameters are greater than ~1 cm. In Section 5 we outline the basic physics of flow in cracks, including scaling relations and order-of-magnitude estimates of derived quantities. In Section 6 we mention some of the consequences of melting. In Section 7 we describe our hydrodynamic model, and in Section 8 we give results. We find that melting is likely unless the crack width is greater than ~10 cm. Since the temperature of the walls responds slowly, the thermal history of the crack is also important. In Section 9 we present conclusions. Several lines of evidence point to multiple cracks per tiger stripe, a conclusion that is testable, in principle.

2. Equilibration of pressures between gas and wall

In this section we show that condensation and evaporation are so rapid that the vapor pressure of the gas is always nearly equal to the SVP of the walls of a tiger stripe or ice pore. From kinetic theory of ideal gases (Jeans, 1954, p. 308), the evaporation rate E from the walls to the gas is

$$E = [e(T) - P](2\pi RT)^{-1/2} \tag{1}$$

Here $e(T)$ is the SVP at the wall temperature T. The equation of state is $e(T) = \rho_v(T)RT$. P is the partial pressure of water vapor in the gas, and $\rho_v(T)$ is the density of the saturated vapor. Eq. (1) is valid when water vapor is the major constituent of the gas phase. The rate is much lower if the vapor has to diffuse through a background gas like nitrogen or carbon dioxide. The above formula does not apply to water vapor in the Earth's atmosphere or water vapor in the Mars regolith, for instance.

To estimate the time needed to establish equilibrium between the gas and the walls, imagine gas in a pore or crack of width δ, roughly equal to twice the pore radius. Take an area of the wall A. Then the volume of the gas is $A\delta$, and its mass is $\rho A\delta$, where ρ is the density of the gas. This mass is increasing at a rate $2EA$, since $2E$ is the mass flux (mass per unit area per unit time) emanating from the two walls on either side of the crack. Eq. (1) thus describes the exponential adjustment of gas density $\rho(t)$ to the saturation vapor pressure of the walls: $d\rho/dt = [e(T) - P]\delta^{-1}(\pi RT/2)^{-1/2}$. It is really the pressure that is adjusting, so we write $d\rho/dt \approx dP/dt\,(RT)^{-1}$, whence

$$\frac{dP}{dt} = \frac{[e_v(T) - P]}{\delta}\left(\frac{2RT}{\pi}\right)^{1/2} \tag{2}$$

According to this equation, the time constant for the adjustment is $\delta(\pi/(2RT))^{1/2}$. Thus the gas and walls equilibrate at sonic speeds. For $\delta = 1$ m and $T = 180$ K (Abramov and Spencer, 2009), this time is 0.0043 s. The time constant is less for narrower cracks, smaller pores, and higher temperatures. Since this time is shorter than any other time constant in the system, we can assume that $P = e(T)$ to a good approximation.

If the fluid is moving steadily upward at velocity v, the left side of Eq. (2) becomes $-v\partial P/\partial z$, where z is depth, increasing downward. If the velocity is equal to $(RT)^{1/2}$, which we will call the thermal speed, the velocity drops out of the left and right sides. Eq. (2) then implies that equilibration occurs in a downstream distance of order $\delta(\pi/2)^{1/2}$. If δ is small compared to the depth of the crack, the pressure of the gas will track the SVP of the walls. If the velocity is equal to $(3RT)^{1/2}$, which is the root mean square molecular speed, the equilibration distance is longer by a factor of $\sqrt{3}$.

The pressures and densities are not exactly equal, however. Small differences will arise between the gas and the ice to accommodate the heat sources and sinks. These small differences can drive large mass fluxes of water between the walls and the gas, so the gas is never far from saturation. Condensation and evaporation occur, but they occur under quasi-equilibrium, i.e., reversible conditions.

3. Heat transport by vapor diffusion

If there is a temperature gradient in the ice, there will be gradients of $e(T)$ and $\rho_v(T)$, and the vapor will diffuse toward the region of lower pressure and temperature. The heat flux F due to vapor diffusion is therefore

$$F = LD\frac{\partial \rho_v}{\partial z} = LD\frac{d\rho_v}{dT}\frac{\partial T}{\partial z} \equiv k_v\frac{\partial T}{\partial z} \tag{3}$$

Here D is the diffusion coefficient for vapor in the pores, and L is the latent heat of vaporization. There is no minus sign because F is the upward heat flux and z is the downward coordinate. Since the pressure in the pores equilibrates instantaneously to the saturation vapor pressure of the icy walls according to Eq. (2), ρ_v is the saturation density at the temperature of the ice, and $k_v = LD(d\rho_v/dT)$ is the effective thermal conductivity for transport by vapor diffusion. Since the vapor is saturated, we use $\rho_v = e(T)/(RT)$, where $e(T) = A\exp(-B/T)$, $A = 3.63\times10^{12}$ Pa, and $B = 6147$ K $\approx L/R$. We chose the numbers A and B by fitting to the vapor pressure of ice (Lide, 1993) from −60 °C to 0 °C. The differences between the fitted curve and the data are less than 3%. Then $d\rho_v/dT = (\rho_v/T)(L/(RT)-1)$. For this discussion, it is sufficient to treat L as a constant equal to 2.8×10^6 J kg^{-1}.

In the Knudsen regime (pore size less than the mean free path), D is roughly equal to the porosity/tortuosity factor ϕ multiplied by the pore radius $\delta/2$ and the thermal speed $(RT)^{1/2}$ of the molecules (Clifford and Hillel, 1983). Therefore $D \approx \phi(\delta/2)(RT)^{1/2}$. The mean free path for water vapor is given by the empirical formula $\Lambda = (1.07\times10^{18}\ \mathrm{m}^{-2})\ (T/300\ \mathrm{K})^{0.6}/n$, where n is the number density of molecules in m^{-3} (Crifo, 1989). The Knudsen regime is important for our problem only if $k_v > 2.4$ W m^{-1} K^{-1}, which is the thermal conductivity for warm ice ($T = 273$ K). The largest value of k_v is obtained with δ as large as possible but still consistent with the Knudsen regime. This means $\delta/2 = \Lambda$. The resulting k_v is a weakly increasing function of T, but even at $T = 273$ K and $\phi = 0.1$, which is the largest realistic value, k_v is 0.23 W m^{-1} K^{-1}. This is an order of magnitude less than the value for warm ice. Therefore the Knudsen regime is not important for our problem. At $T = 273$ K, the value of Λ is 6.2 μm. At 200 K, it is 14 mm.

In the viscous flow regime (pore size greater than the mean free path), the balance is between the pressure gradient force and the viscous force tending to oppose it. For laminar flow in a tube of diameter δ, the mass flux in the tube (mass per unit area per unit time) is $\rho_v\delta^2/(32\eta)(\partial P/\partial z)$, where η is the dynamic viscosity of the gas. Multiplying by the porosity/tortuosity factor ϕ converts this into the average mass flux in the matrix, and multiplying by the latent heat L converts it into a heat flux F. Thus, in the viscous flow regime,

$$F_v = L\phi\frac{\rho_v\delta^2}{32\eta}\frac{\partial P}{\partial z} = L\phi\frac{\rho_v\delta^2}{32\eta}\frac{\partial P}{\partial T}\frac{\partial T}{\partial z} \equiv k_v\frac{\partial T}{\partial z} \tag{4}$$

The effective thermal conductivity is proportional to the square of the SVP through the factors $\rho_v = e(T)/(RT)$ and $\partial P/\partial T = e(T)(L/(RT^2))$, which is the ideal gas approximation to the Clausius Clapeyron equation. An empirical formula for the dynamic viscosity of water vapor is $\eta = 0.925\times10^{-5}\ (T/300)^{1.1}$ Pa s (Crifo, 1989). With this formula and $e(T) = A\exp(-B/T)$ one can show that

$$F_v = \left(1 - \frac{2.1\ RT}{2\ L}\right)^{-1}\frac{\partial Y}{\partial z} \approx \frac{\partial Y}{\partial z}, \quad Y(T) \equiv \frac{L\phi\rho_v P\delta^2}{64\eta} \tag{5}$$

This equation holds because the vapor is saturated. It says that the vapor heat flux is proportional to the gradient of Y, which plays the role that kT does when the thermal conductivity k is constant. We verified that the flow is laminar using the formula for the velocity $v = \delta^2/(32\eta)(\partial P/\partial z)$. Even for $\delta = 1$ cm and pressures of order 600 Pa varying by factors of 2 over a distance of 100 m, the Reynolds number $\rho v\delta/\eta$ is less than 10.

Turcotte and Schubert (2002) give an idealized model for the relation between pore diameter δ, porosity/tortuosity ϕ, and grain size b, assuming long thin pores (tubes) of cylindrical cross section. Their Eqs. (6)–(9) says $\delta^2 = 0.4b^2\phi$, whence $Y(T)$ becomes

$$Y(T,\ \phi b) \equiv \frac{L\rho_v P(\phi b)^2}{160\eta} \tag{6}$$

The dependence on T is through ρ_v, ρ, and η; the dependence on matrix properties is through ϕb. We apply Eqs. (5) and (6) to Enceladus in the next section.

4. Vapor diffusion on Enceladus

The total power radiated from the South Polar Region, in excess of the power absorbed from sunlight, is 5.8 ± 1.9 GW (Spencer et al., 2006; Abramov and Spencer, 2009), which converts to 11.6 ± 3.8 kW m^{-1}, on average, along the 500 km length of the tiger stripes. The amount of water vapor escaping from Enceladus in the plumes is 250 ± 100 kg s^{-1} (Hansen et al., 2006, 2008), which represents 0.7 GW of latent heat for the latent heat of vaporization $L = 2.8\times10^6$ J kg^{-1} of cold ice. This converts to 1.4 kW m^{-1}, on average, along the 500 km length of the tiger stripes. Thus the average power lost per unit length Q is the sum 11.6 + 1.4 = 13 kW m^{-1}, of which 10% is latent heat and 90% is radiation. These numbers vary from place to place along the tiger stripes, so the local power per unit length can be significantly greater than the average.

In this section we assume $F_{tot} = k_{ice}\partial T/\partial z + \partial Y/\partial z$, which means that heat transfer is by thermal conduction and vapor diffusion. In subsequent sections we discuss open cracks and heat transfer by hydrodynamic flow. The conduction/diffusion assumption applies both to the Gioia et al. (2007) model and to the ductile zone of the Nimmo et al. (2007) model. Thus in the Gioia et al. model, Q is the full heat flux of 13 kW m^{-1}. In the Nimmo et al. model, Q is the part of the heat flux that is generated in the ductile zone, since the part that is generated in the brittle zone can flow out as vapor through the open crack. For the parameters listed in Fig. 1 of Nimmo et al. (2007) the heat generated in the brittle zone is 2 kW m^{-1} and the heat generated in the ductile zone is ∼10 kW m^{-1}. In what follows we take $Q = 12$ kW m^{-1} as the average for the Nimmo et al. ductile zone and the Gioia et al. cracked material.

We first consider a highly idealized model with constant heating q (power per unit volume) inside a long, buried, horizontal cylinder of radius r_0. The axis of the cylinder is a horizontal line at depth d, with $d \geqslant r_0$. This crudely approximates the heating in the ductile zone in the Nimmo et al. (2007) model, where the maximum heating is near the base of the crack ($z = d$), at the brittle–ductile transition. The integral of q over the cross-sectional area of the cylinder is Q, so that $q = Q/(\pi r_0^2)$. We use Eq. (5) and we assume k_{ice} is constant, so that the dependent variable is $\psi = k_{ice}T + Y$, and it obeys the steady-state diffusion equation

$$\nabla^2\psi \equiv \nabla^2(k_{ice}T + Y) = \begin{cases} q, & r \leqslant r_0 \\ 0, & r > r_0 \end{cases} \tag{7}$$

The boundary condition is $\psi = \psi_0 = k_{ice}T_s$ at $z = 0$, where $T_s = 72$ K is a characteristic surface temperature at the south pole at solstice. This assumes $Y = 0$ at the surface, which is a good assumption at temperatures of order 72 K. This boundary condition on ψ allows us to use the method of images, which involves adding a cooled cylinder above the surface (depth = $-d$) to offset the heated cylinder at depth d. Thus

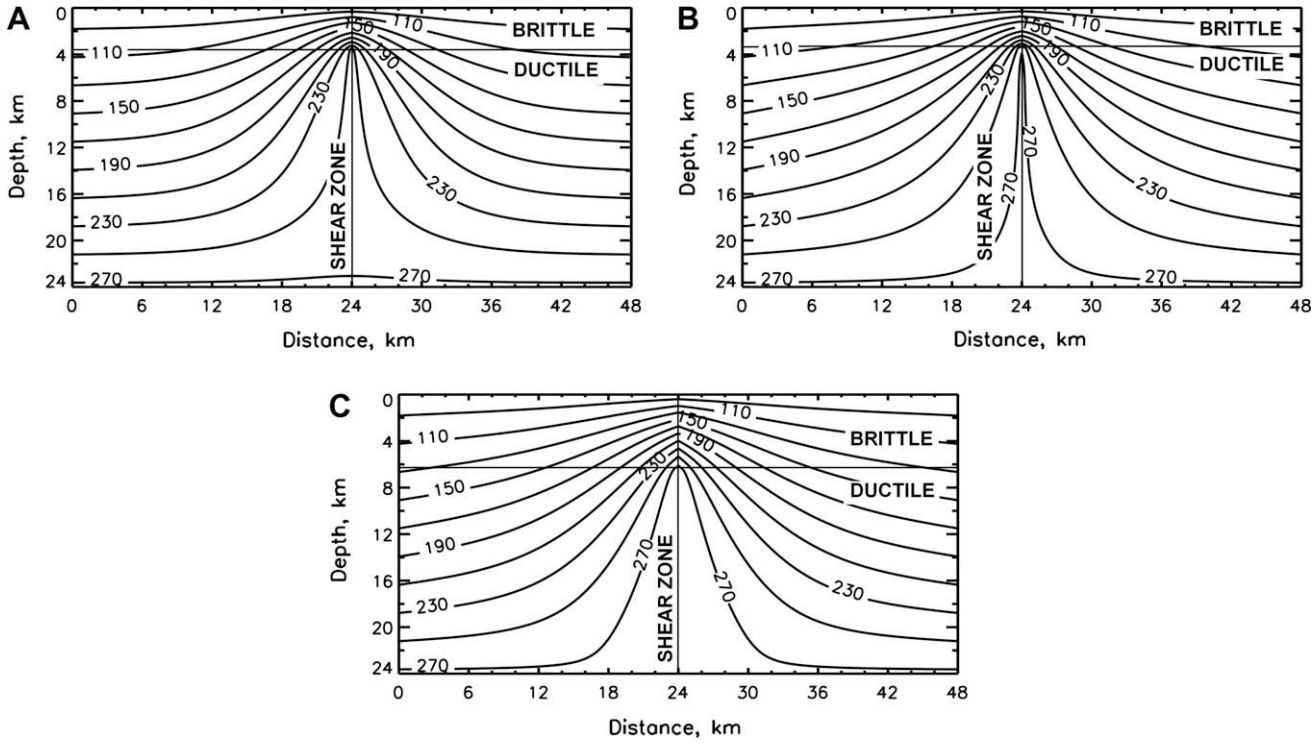

Fig. 1. Temperature distribution near a shear zone. This is our version of Fig. 1 of the paper by Nimmo et al. (2007). The main difference is that we require that the vapor pressure in the pores be equal to the saturation vapor pressure (SVP) of the surrounding ice. As a result, the thermal conductivity is less than that in the calculations by Nimmo et al. The ice in our model is warmer, the viscosity is lower, and the heat generated is less. (A) Our model with the same values as described in the caption to their figure: shear velocity = 8×10^{-6} m s^{-1}, coefficient of friction $f = 0.3$, ice density = 920 kg m^{-3}, ice reference viscosity 10^{13} Pa s, constant thermal conductivity, and temperature-dependent viscosity as described in their paper. (B) Same, except the reference viscosity is 10^{14} Pa s. (C) Same, except the reference viscosity is 10^{15} Pa s.

$$\psi(\vec{r}) - \psi_0 = \int \frac{q(\vec{r}')}{2\pi} \log\left(\frac{|\vec{r} - \vec{r}'|}{|\vec{r} - \vec{r}''|}\right) dA' \tag{8}$$

Vectors in this equation are two-dimensional and lie in a vertical plane perpendicular to the axis of the cylinder. $\vec{r}'$ is the position vector corresponding to a small area dA' in the vertical plane, and $\vec{r}''$ is its mirror image reflected in the plane $z = 0$. We evaluate the integral at the warmest place, which is at depth d, on the axis of the cylinder, and call the result $\psi(d)$. Then $(\psi(d) - \psi_0)/Q$ depends only on the ratio d/r_0. When the ratio is large, the heated cylinder is thin and far from the surface. When the ratio is unity, the cylinder is wide and touches the surface.

For $d/r_0 = 1, 2, 4$, and 8, the values of $(\psi(d) - \psi_0)/Q$ are 0.19, 0.30, 0.41, and 0.52, respectively. The value for $d/r_0 = 2$ is probably the closest to the Nimmo et al. model, since it gives heating in the ductile zone spread out vertically between $z = 0.5d$ and $z = 1.5d$. Thus we can use Eq. (6) with $[\psi(d) - \psi_0]/Q \approx 0.3$ to find a lower bound on ϕb necessary to prevent melting. The equation becomes $Y(T_d,\ \phi b) + k_{ice}(T_d - T_s) = 0.3Q$. The temperature at depth d is T_d, which we take to be $\leqslant 273$ K if melting is to be avoided. With $Q = 12$ kW m^{-1}, the result is $\phi b \geqslant 9 \times 10^{-4}$ m. With these values, possible porosity/grain size combinations include $(\phi,\ b) \geqslant (0.1,\ 0.9$ cm) and $(\phi,\ b) \geqslant (0.01,\ 9$ cm). In other words, the matrix must be a rubble pile. Higher values of Q, which are appropriate if the heat flux varies along the tiger stripe, require even larger grain sizes and porosities to avoid melting. In this calculation, the precise value of $\psi_0 \equiv k_{ice}T_s$ is unimportant since ψ_0 is small compared to $0.3Q$.

Since the value of Q is not too different for the ductile zone in the Nimmo et al. model and the cracked conduits in the Gioia et al. model, both models lead to the same conclusion: the ice will melt unless it is a rubble pile. A rubble pile at depths of 4 km requires some gardening, because the grains tend to collapse under the hydrostatic load. The time to collapse is the dynamic viscosity divided by the hydrostatic pressure (e.g., Crawford and Stevenson, 1988), which for ice at 4 km depth (the depth to the ductile zone in the Nimmo et al. model) is 4×10^5 Pa. The dynamic viscosity depends on the grain size, which is unknown, but for warm ice it is in the range 10^{13}–10^{15} Pa s (Goldsby and Kohlstadt, 2001; Nimmo and Gaidos, 2002). Therefore the time to collapse is of order 1–100 years. The time would be longer if the ice were colder, but this is unlikely because cold ice cannot carry the observed heat—the thermal conductivity due to vapor diffusion is proportional to the SVP squared according to Eq. (4). The cold ice will heat up when subjected to a subsurface heating rate Q of 12 kW m^{-1}. Sublimation might help keep the pores open, but condensation might help close them. In view of the large uncertainties, a thorough discussion of pore size is beyond the scope of this paper.

There might be a way to avoid melting, even with non-porous ice, and that is to have multiple cracks that share the heat flux Q among them. Non-porous ice implies $\phi b = 0$ and $Y = 0$, so that $\psi \equiv k_{ice}T$. Heat transfer is entirely by conduction through the ice. The conductivity of the ice and its temperature dependence both matter, but we get a crude estimate by taking k_{ice} = constant ≈ 2.4 W m^{-1} K^{-1}, a value appropriate to ice at 273 K (Lide, 1993). The image solution $[\psi(d) - \psi_0]/Q \approx 0.3$ becomes $k_{ice}[T_d - T_s] \approx 0.3Q$. With $T_d \leqslant 273$ K to avoid melting, and $T_s = 72$ K, the value of Q in the ductile zone must be $\leqslant 1.6$ kW m^{-1}. Combining this with the 2 kW m^{-1} that is generated in the brittle zone in the Nimmo et al. model, one would need three or four cracks per tiger stripe to supply the observed radiated power of 11.6 kW m^{-1}. That avoids melting only if the horizontal separation of the cracks is comparable to their vertical dimension. If they are packed closer than this, their heat fluxes will blend and the effect on the ice will be the same as one crack that generates 11.6 kW m^{-1}. The Cassini spacecraft should be able to see three or four cracks separated from each other by several km. If multiple

cracks are not seen, the other possibilities are that the heat in the brittle zone is greater than 2 kW m^{-1}, that melting does occur in the ductile zone, and that the ductile zone is a rubble pile.

Fig. 1A shows a more careful calculation that gives the same result. This is our version of Fig. 1 of the Nimmo et al. (2007) paper. With one exception, the parameter values are the same as described in the caption to their figure: shear velocity = 8×10^{-6} m s^{-1}, coefficient of friction $f = 0.3$, ice density = 920 kg m^{-3}, ice reference viscosity 10^{13} Pa s, constant thermal conductivity $k_{ice} = 3$ W m^{-1} K^{-1}, and temperature-dependent viscosity as described by Nimmo et al. (2007). The depth of the brittle zone is calculated self-consistently from stresses in the brittle and ductile zones. The one difference between our model and the Nimmo et al. (2007) model is in the treatment of heat transfer by vapor diffusion through porous ice. Nimmo et al. (2007) assume that the vapor carries 90% of the heat that is generated, both in the ductile zone and in the brittle zone. This is a reasonable assumption for the brittle zone, since a wide enough crack can carry away the heat. However, in the ductile zone, where there are no open cracks, heat transport by the vapor is negligible, especially for the porosity/grain size combinations used by Nimmo et al. (2007), because the vapor pressure is low. Therefore we assume that the heat generated in the ductile zone is carried away solely by thermal conduction in the ice. As a result, the temperature in our model is warmer than in their model. This lowers the viscosity in the ductile zone, and less heat is generated, but all of it goes into heating the ice, rather than just 10% as in Nimmo et al. (2007). In Fig. 1A, we find that the temperature is 250 K at the brittle–ductile boundary 3.5 km below the surface. The heat generated in the ductile zone is 1.7 kW m^{-1}. With this value of the heat flux, the ice is close to melting at the bottom of the ductile zone. This agrees with the condition derived from our image solution, that Q in the ductile zone must be less than 1.6 kW m^{-1} to avoid melting, if heat transfer is by thermal conduction alone.

Heat from the brittle zone provides an additional 1.5 kW m^{-1}, according to the model of Fig. 1A. If all the heat from the ductile and brittle zones goes into radiation at the tiger stripes, one would still need three or four widely separated cracks per tiger stripe to match the observed 11.6 kW m^{-1} of radiated power.

Fig. 1B and C shows the same calculation but with larger values of the reference viscosity: 10^{14} Pa s and 10^{15} Pa s, respectively. The reference viscosity is defined as the value at $T = 250$ K. In Fig. 1A its value is 10^{13} Pa s. In all three parts of Fig. 1 we assume the viscosity decreases with increasing temperature (Nimmo et al., 2007; Mitri and Showman, 2005) and drops sharply near 273 K as in Nimmo et al. (2007) to simulate the effect of pre-melting (Goldsby and Kohlstadt, 2001). In Fig. 1B, the depth of the crack and the heat fluxes in the ductile and brittle zones are the same as in Fig. 1A. In Fig. 1C the heat fluxes in the ductile and brittle zones are 3.6 kW m^{-1} and 5.3 kW m^{-1}, respectively. Given the uncertainties, if all this heat goes into radiation, one crack could probably supply the observed 11.6 kW m^{-1} of radiated power in the model of Fig. 1C. Melting, however, is still a possibility.

In Fig. 1B, the 273 K isotherm extends almost up to the base of the brittle zone at $d = 3.5$ km. Also, the high temperatures are concentrated closer to the shear zone than in Fig. 1A, and the temperatures along the fault are higher. In Fig. 1C, melting occurs at the brittle–ductile boundary, and the area in the ductile zone where melting occurs is more extensive than in Fig. 1B. In our model, the depth of the crack is the shallowest of two levels the one where melting occurs and the one where the stresses in the brittle and ductile zones are equal. In Fig. 1C melting occurs at 6.4 km and the stresses are equal at 6.5 km, so the depth of the crack is at 6.4 km. When melting occurs, we set the viscosity equal to the viscosity of ice at 273 K, with the effect of pre-melting included, and we assume that the excess heat goes into melt production as in Nimmo and Gaidos (2002). This is an approximation, because the viscosity will probably continue changing beyond the limits of the pre-melting approximation in the presence of melted water, as will the coefficient of friction. Thus melting is likely, but what happens after that is beyond the scope of this paper.

5. Flow in cracks: scaling relations

Although hydrodynamic flow in an open crack is an efficient form of heat transfer, size matters. Wide cracks transport heat more effectively than narrow cracks. For a crack of width δ with vapor flowing upward at the thermal speed $(RT)^{1/2}$, the power per unit length of the crack is the mass flux times $L\delta$, or $L\delta\rho_v(T)(RT)^{1/2} = L\delta e(T)(RT)^{-1/2}$, where $\rho_v(T)$ and $e(T)$ are the density and pressure of the saturated vapor. For $\delta = 1$ m and $T = 180$, 210, and 240 K, the power per unit length is 0.052, 6.3, and 230 kW m^{-1}, respectively. These numbers bracket the average radiated power per unit length Q, which is 12 kW m^{-1}, assuming the 6 GW is distributed along the 500 km cumulative length of the tiger stripes. For a 1 m crack, walls colder than about 210 K cannot carry the observed heat flux. If the upward velocity were twice as large, $2(RT)^{1/2}$ instead of $(RT)^{1/2}$ (Tian et al., 2007), the critical temperature would be 205 K instead of 210 K, a negligible difference because the SVP is such a steep function of T. For $\delta = 2$ mm, T would have to be 276 K to supply 12 kW m^{-1} to the surface layers. If the cracks are this narrow, one can expect melting at depth. On the other hand, if there are several cracks per tiger stripe separated by several km or more, each crack has to supply only a fraction of the 12 kW m^{-1}, and the temperatures will be lower. Abramov and Spencer (2009) give one example. Their Fig. 4 shows two adjacent pixels, each 6 km wide, which they call Regions 5 and 6. A large fracture runs down the middle of Region 5, but no large fracture is apparent in Region 6. The spectrum of the former is best fit with a fracture temperature of 223 K and that of the latter with a fracture temperature of 195 K. In reference to Region 6 they remark, "perhaps a smaller active feature is present in this region."

The crack width has not been measured. Simple scaling arguments (Crawford and Stevenson, 1988) say that a tensional stress τ should produce a crack width of order $\tau d/\mu$, where $\mu = 4$ GPa is the shear modulus of ice and d is the depth to which the crack extends. Tides on Enceladus have $\tau \sim 100$ kPa (Hurford et al., 2007; Nimmo et al., 2007), which gives $\delta \sim 10$ cm when $d = 4000$ m. The latter is an estimate of the brittle–ductile transition depth for the model in Fig. 1A, below which the ice flows and does not break. The width δ would be greater than 10 cm if cracking had weakened the ice, because that would give a smaller μ.

A high-pressure gas erupting into a low-pressure environment is a classic fluid dynamics problem, with applications ranging from rocket nozzles and the solar wind to volcanoes and geysers. In ideal cases the gas can convert all of its initial enthalpy C_pT into kinetic energy (Landau and Lifshitz, 1959, p. 316). The specific heat C_p of water vapor is 1850 J $(kg\ K)^{-1}$, which is almost exactly four times the gas constant R for water vapor. Thus the plumes could theoretically reach speeds of $(2C_pT)^{1/2} = 816$ and 1005 m s^{-1} for $T = 180$ and 273 K, respectively.

On time scales of order milliseconds, the pressure of the gas adjusts to that of the walls. However on longer time scales, the walls adjust to the cooling/heating $L * E$ (latent heat times the evaporation rate). To estimate this time scale, treat each wall as an isothermal conductor that is suddenly subjected to a heat flux F. The wall surface warms by an amount ΔT in a time Δt according to the formula $F = \Delta T(k\rho C/\Delta t)^{1/2}$. The quantity $(k\rho C)^{1/2}$ is called the thermal inertia, k is the thermal conductivity, ρ is the density, and C is the specific heat of the ice. For ice at 220 K, $k = 3.0$ W $(K\ m)^{-1}$, $\rho = 917$ kg m^{-3}, and $C = 1600$ J $(kg\ K)^{-1}$. If a meter-sized crack

opened up in ice at 72 K, it would have to warm at least to 210 K, as described above, before the vapor were capable of carrying a significant fraction of the 6 GW distributed along the 500 km length of tiger stripes. Thus $\Delta T \geqslant 138$ K. Assuming the energy source is at a depth of 1 km or more, the heat flux F is no more than 6 GW divided by the area of the walls, which is 2×500 km $\times$ 1 km. The factor of 2 arises because there are two walls. This gives $F \leqslant 6$ W m^{-2}. This heat flux can warm the walls by 135 K in a time $\Delta t \geqslant k\rho C(\Delta T/F)^2 = 67$ years. This is the time needed to establish a plume starting from a fracture in cold ice. The time needed for the ice to come into *complete* thermal equilibrium, i.e., with the heat source, with conduction to the surface, and with evaporation/condensation in the crack—varies with depth as z^2/κ, where $\kappa = k/(\rho C)$ is the thermal diffusivity of ice. For $z = 10$ m this time is 2 years, and for $z = 100$ m the time is 200 years.

Cracks tend to close up as water condenses on the walls. Surface temperatures of 180 K or more are observed near the cracks (Spencer et al., 2006; Abramov and Spencer, 2009), and this heat has to be conducted through the ice from below. The heat flux F_{IR} from a 180 K blackbody is $\sim$60 W m^{-2}, and most of this heat flux is supplied by condensation on the walls of the crack at shallow depths, i.e., at depths comparable to the width. This is because the path length for conduction through the ice is smallest for the shallowest depths. The deposition rate v_{ice} (meters of ice per second) on each wall is therefore of order $F_{IR}/(\rho_{ice}L)$, where L is the latent heat of vaporization for gas or the latent heat of fusion for liquid. For the gas, the rate is 0.8 m year^{-1}, and for the liquid the rate is 5.5 m year^{-1}. The latter is seven times greater than the former because the latent heat of fusion is that much less than the latent heat of vaporization. These rates seem to imply that the cracks seal themselves off in 1 year or less. However, if the crack is 1 m wide, most of the deposition is happening in the upper few meters of the crack. It is possible that the daily opening and closing of the cracks grinds this frost away, leaving it to fall back into the crack. Such self-cleansing does not happen if the fluid in the crack is liquid, because the frost will float on the surface. It is also possible that the surface is changing on space and time scales of meters and years, as the place where a deep crack opens to the surface shifts its location.

6. Effects of liquid water

Melting has a drastic effect on the heat budget. If the heat is generated by viscous shear in the ice, as in the Nimmo et al. (2007) model, then melting will reduce the viscosity by many orders of magnitude, from that of warm ice to that of liquid, effectively shutting off the heat source. Melting will create liquid-filled pores. The melt, which is more dense, might drain downwards (Gaidos and Nimmo, 2000), or if it reaches a subsurface ocean it will adjust to a height that is 92% (the ratio of ice density to liquid water density) of the distance from the ocean to the surface of Enceladus. In that case the hydrostatic pressure will hold the pores open, i.e., they will not collapse, as vapor-filled pores might. In the Nimmo et al. (2007) model, where the subsurface ocean is at a depth of 24 km, the water table will adjust to a depth 1.9 km below the surface. This is the equilibrium depth of the liquid surface.

Heat loss to the ice could impede this adjustment. The discussion in the last section, of the time needed to establish flow to the surface in cold ice, applies equally well if the fluid is liquid. The statement $\Delta t \geqslant k\rho C(\Delta T/F)^2 = 67$ years, depends on the heat flux and the thermal inertia of the ice, but it does not depend on the properties of the fluid. Liquid water cannot rise to its equilibrium height until the walls are warm enough. The heat flux F determines the rate at which the walls warm up, and that rate is the same whether the fluid is liquid or vapor.

Friction with the walls also impedes this adjustment. For laminar viscous flow in a narrow crack, the velocity profile is a parabola and the mean velocity $\bar{v}$ is 2/3 the maximum velocity. The viscous stress on each wall is $6\eta\bar{v}/\delta$, and the dynamic viscosity η of liquid water at 0 °C is 1.8×10^{-3} Pa s (Lide, 1993). If the total height of water in the crack is h, then the total viscous force per unit length along the tiger stripe is $12\eta\bar{v}h/\delta$, and it is downward if $\bar{v}$ is upward. This force is balanced by an upward force per unit length $\rho g\Delta z\delta$, where Δz is the depth of the water table below its equilibrium height. To carry the heat flux Q, the fluid must flow upward at speeds $\bar{v}$ of order $Q/(\rho L\delta)$, where L is the latent heat of fusion if the fluid is liquid water. Therefore the depth of the water table below equilibrium is

$$\Delta z = 12\eta hQ/(\rho^2 gL\delta^3) \tag{9}$$

For $\eta = 1.8 \times 10^{-3}$ Pa s, $h = 20$ km, $Q = 12$ kW m^{-1}, $\rho = 10^3$ kg m^{-3}, $g = 0.11$ m s^{-2}, $L = 3.3 \times 10^5$ J kg^{-1}, and $\delta = 1$ cm, the water table is depressed by 143 m. For $\delta = 0.5$ cm, it is depressed by 1.1 km. If the cracks are even narrower than these values, the liquid water cannot get close to the surface and still deliver the observed heat flux.

A liquid will boil if two conditions are met: the SVP must exceed the ambient pressure, and bubbles must be able to nucleate in the liquid. On Enceladus, the first condition is met down to a depth 5.6 m below the water surface, if the water is at 0 °C and the water surface is exposed to vacuum. This is the depth at which the hydrostatic pressure is equal to the 611 Pa pressure of the vapor at 0 °C. The second condition is met at temperatures above a certain critical temperature, which may be greater than 0 °C, by homogeneous nucleation (Brilliantov et al., 2008). Impurities can lower the temperature at which nucleation occurs. Freezing lowers the SVP of the upper frozen layers and insulates the liquid below, thereby reducing the tendency to boil. On the other hand, tidal stresses might crack the ice and expose the liquid to vacuum, and boiling might resume. Further discussion of melting, liquid water, and boiling on Enceladus is beyond the scope of this paper.

7. Hydrodynamic model: details

Flow of vapor in an icy crack is an effective way to transport heat, but there must be a way for the heat to reach the crack. In earlier sections we considered conductive and diffusive heat transport and showed that temperatures around the source region can reach the melting point unless the porosity and grain size are large. In these sections we consider heat transport in an open crack, with two variations. The first is where the base of the crack is connected to the heat source and erupts with the full power per unit length Q required by the observations. The second is where the heat is generated by friction on the walls of the crack, as in the brittle zone of the Nimmo et al. (2007) model. That heat goes into evaporation, and the vapor carries the heat to the surface. We present the details of the model in this section and the results in the next section.

The following steady-state equations express the conservation of mass, momentum, and energy:

$$-\frac{\partial(\rho v\delta)}{\partial z} = E \tag{10}$$

$$-\rho v\delta\frac{\partial v}{\partial z} - \delta\frac{\partial P}{\partial z} = -\rho g\delta - \tau - vE^* \tag{11}$$

$$-\rho v\delta\left(C_v\frac{\partial T}{\partial z} - L\frac{\partial s}{\partial z}\right) - P\delta\frac{\partial v}{\partial z} = \frac{P}{\rho}E + Pv\frac{\partial\delta}{\partial z} + LsE - \left(E^* + \frac{\tau}{v}\right)C_V\Delta T + \frac{v^2}{2}E^* + v\tau \tag{12}$$

The upward velocity is v and the downward coordinate is z. With the minus sign on the left, E is the flux of mass from the walls into the flow, and τ is the downward stress of the walls on the flow.

The three dependent variables, which are functions of z only, are T, v, and s, where s is the mass of suspended solids per unit mass of the mixture. The width of the crack is δ, which is a function of z. The pressure P is the SVP at the temperature of the walls, and we use the approximate formula $e(T) = A\ \exp(-B/T)$. The density of the vapor is ρ_v, which is computed from the ideal gas law $e(T) = \rho_v RT$, where R is the universal gas constant divided by the molar mass of water. The volume of the suspended solids is negligible, so the density ρ of the mixture is $\rho_v/(1-s)$. The latent heat of vaporization L is treated as a constant of magnitude 2.8×10^6 J kg^{-1}. The specific heat of the mixture at constant volume is also treated as a constant, $C_v = 2000$ J kg^{-1} K^{-1}. The gravitational acceleration g is 0.11 m s^{-2}. We assume the mixture has no latent heat when the water is in the vapor phase, but it has negative latent heat in the solid phase. Thus the latent heat per unit mass is $-Ls$, where s is the mass fraction of solid in the mixture. If we had assumed the mixture has no latent heat in the solid phase, the latent heat per unit mass would be $L(1-s)$ and the results would be the same.

Eq. (10) is in flux form—the left side is the divergence of the downstream mass flux. Eqs. (11) and (12) are in advection form—the left sides are the rates of increase of momentum and internal energy, respectively, of average parcels in the flow. As a check, we derived Eqs. (11) and (12) in two ways, one from the advection forms shown here and the other from the flux forms for downstream momentum and total energy (kinetic, internal, and gravitational), respectively.

The three terms on the right of Eq. (11) are positive upward forces per unit area, and they are all negative. We define $E^* = E$ when $E > 0$, and $E^* = 0$ when $E < 0$. The first term on the right of (11) is gravity. The second term is stress (force per unit area) of the walls on the flow. The third term is advection of momentum during evaporation: When $E > 0$, we are adding fluid with zero momentum to the flow, so the average momentum of the flow decreases. When $E < 0$, the average momentum of the flow does not change.

The terms on the right of (12) are the rate of increase of internal energy by average parcels in the flow. The first two terms are work done on the fluid by the pressure force when the flow is contracting, either by evaporation from the walls (the first term is a contraction when $E > 0$) or by downstream contraction of the channel (the second term is a contraction when $\partial\delta/\partial z > 0$). The third term is gain of latent heat during evaporation ($E > 0$), assuming evaporation adds vapor but no particles to the flow. The fourth term is cooling when $\Delta T = (T - T_{wall}) > 0$, that is, when cold fluid evaporating from the walls mixes with warmer fluid in the channel. The fifth term is cooling due to turbulent or conductive heat transfer between the walls and the flow. We use the same effective mass flux τ/v for heat as we do for momentum. The sixth and seventh terms represent dissipation, that is, the gain of internal energy that occurs when kinetic energy is turned into heat. The sixth term is the dissipation due to evaporation, when stationary fluid from the walls mixes with moving fluid in the channel. The seventh term is the dissipation due to friction.

To solve the equations, we do the differentiation on the left side of (10). The derivative $\partial\rho/\partial z$ produces a term proportional to $\partial T/\partial z$ and a term proportional to $\partial s/\partial z$, since $\rho = \rho_v(T)/(1-s)$. Terms that do not involve the derivatives $\partial T/\partial z$, $\partial v/\partial z$, and $\partial s/\partial z$ are moved to the right side. The 3×3 system of algebraic equations is solved for the three derivatives; the right sides are linear combinations of E, g, τ, and $\partial\delta/\partial z$. The three equations are integrated numerically starting from initial conditions $T = T_d$, $v = v_d$, and $s = s_d$ at $z = d$. We consider cases where v_d and s_d are zero and other cases where they are not zero.

The evaporation rate E (mass of water per unit time per unit area on the walls) is given by $E = (F_s - F_c)/L$, where F_s is the frictional heating on the walls of the crack and F_c is the heat conducted into the ice. In cases where the flow erupts from a deep reservoir, $\rho_v v_d L\delta$ is equal to Q, and F_s is zero. In cases where the heating is on the sides of the crack, v_d is zero and the integral of F_s with respect to z is Q. In most of the latter cases, we give F_s the form $F_s = 12(z/d)Q[1-(z/d)^{10}]/(5d)$. That function increases almost linearly for $0 < z < 3d/4$ and falls rapidly to zero at $z = d$. This avoids a discontinuity in the solutions at $z = d$ brought on by having a finite heat flux and zero velocity. We also considered cases where F_s is almost constant and then falls rapidly to zero in the region $3d/4 < z < d$. The results are not sensitive to the distribution of heating or whether the flow erupts from a deep reservoir or from the walls.

To reduce the problem to one dimension, we use a parameterized formulation for F_c, which is twice the conductive heat flux on one side of the crack. For large z the formula is $F_c = F_1 = 4k_{ice}(T - T_s)/(\pi z)$, where k_{ice} is the thermal conductivity of ice at 220 K, about 3 W m^{-1} K^{-1}, and T_s is the temperature of the surface. This is the exact steady-state solution for an infinitely deep vertical crack at temperature T that intersects an infinitely wide horizontal surface at temperature T_s, when both T and T_s are constant. This formula has a singularity at $z = 0$, which arises because of the discontinuity in temperature where the planes intersect. In reality, the temperature of the crack close to the surface will decrease, and the temperature of the surface will increase so as to eliminate the discontinuity. The formula then has a 0/0 indeterminacy as $z \to 0$, which is resolved in our model by requiring that the heat flux F_c approach $F_2 = \sigma T^4 - \sigma T_s^4$, where T_s is the 72 K background temperature at the surface. This blending is accomplished with the formula $F_c = F_1 F_2/(F_1 + F_2)$. We checked this parameterization by solving the two-dimensional heat flow equation in the ice at steady state and found it was accurate to ±15% within several hundred meters from the surface and to <1% at larger depths. Overall, F_c has a small effect: Doubling k_{ice} causes a 2 K decrease in T, and halving it causes a 1 K increase. For $T = 228$ K, the crossover point, where $F_1 = F_2$ is 3 m below the surface.

The power per unit length Q_{vap} that leaves the vent as latent heat of vaporization is $\rho_v v L\delta$, evaluated at the surface $z = 0$. This power is less than the power per unit length Q that enters the crack. The remaining power, $Q - \rho_v v L\delta \equiv Q_{rad}$, is conducted into the ice and finally lost to space by radiation. What happens at horizontal distances less than or equal to the vent width is uncertain, however. Some of the power $\rho_v v L\delta$ carried with the vapor is coming straight out of the vent, and the rest is coming from the evaporation of warm surface ice that is close to the vent. The partitioning depends on the shape of the vent and the temperatures within one vent width away from the vent. We experimented with different boundary conditions, in particular the function F_2 defined in the preceding paragraph, and found that $\rho_v v L\delta$ is a fairly robust estimate (error ±4%) of the total power carried with the vapor, although the partitioning between vaporization in the vent and vaporization on the surface is uncertain. In almost all cases the former is at least twice as large as the latter. See Abramov and Spencer (2009) for further discussion of this problem.

The wall stress τ is the drag force per unit area due to the two walls, and is either $12\eta v/\delta$ or $2C_d\rho_v v^2$, whichever is larger. The first expression is due to viscous drag. We derived this formula assuming laminar flow between no-slip planar boundaries separated by a distance δ. The velocity profile is a parabola with zero velocity on the boundaries; the mean velocity v is 2/3 the velocity at the mid-plane, and the velocity gradient at the wall is $6v/\delta$. The second expression is due to turbulent drag. Here C_d is the drag coefficient, to which we assign the value 0.002 (Arya, 1988). For the dynamic viscosity of water vapor we used $\eta = 0.925 \times 10^{-5}\ (T/300)^{1.1}$ Pa s (Crifo, 1989). Instead of simply adding the viscous drag and the turbulent drag, we combined the sum of squares and took the square root. This made the transition from viscous drag to turbu-

lent drag more abrupt. The two terms are equal when the Reynolds number $Re = \rho v \delta/\eta$ is equal to $6/C_d = 3000$. Since $\rho_v v \delta$ is of order Q/L and η is of order 0.75×10^{-5} Pa s, the Reynolds number is always in the range 250–750 and the viscous term is always the largest. We use the same effective mass flux normal to the surface τ/v for heat as for momentum, assuming diffusive processes are the same for the two quantities. ($\tau/(\rho v)$ is sometimes called the piston velocity.)

In computing $T(z)$, $v(z)$, and $s(z)$ we assumed that the gas and particles are thermally and mechanically coupled. The mixture obeys equilibrium thermodynamics. A large number of small particles—a mist—would behave in this way if there were an adequate number of nucleation sites. When s starts to go negative, we interpret any further decrease in Ls as an increase in sensible heat $C_v T$ of the vapor, which balances the left side of Eq. (12). This leads to a condition where $T > T_{wall}$ and the gas is unsaturated. In practice, $T - T_{wall}$ is never greater than 2 K. It can never be negative, because the pressure of the gas is the SVP of the wall, and the gas is not allowed to become supersaturated. By assuming the particles move with the gas and have the same temperature as the gas, we are probably overestimating the particle speed and the mass fraction s. Our treatment of particles forming in a gas that is interacting thermodynamically with the walls is preliminary and needs further work. Schmidt et al. (2008) discuss supersaturation, particle size, and nucleation for a gas that does not interact thermodynamically with the walls.

The solutions of Eqs. (10)–(12) are fully equilibrated, meaning that the flow and the ice are both in steady state. The ice is conducting heat from the walls to the surface, and the flow is transporting heat from the depths to near the surface. In finding the solution we search for the minimum starting temperature $T_d \equiv T(d)$ for which the solution does not blow up. Blowing up happens when velocity reaches the sound velocity of the saturated vapor before the integration reaches the surface at $z = 0$.

There is some inconsistency in presenting fully equilibrated solutions, since deposition on the walls appears to be changing the shape of the crack faster than the temperature can adjust. However the adjustment time varies with depth as z^2/κ, as shown earlier, where z is the depth and $\kappa = k/(\rho C)$ is the thermal diffusivity of ice. For $z = 10$ m this time is 2 years, and for $z = 5$ m it is 0.5 years. The crack is sealing itself off in ~1 year in the upper 1 or 2 m. Since the temperatures there can adjust to the changing position of the crack, the fully equilibrated solutions are not unreasonable. Solving a time-dependent model over the complete life cycle of a crack introduces many new parameters and is also beyond the scope of this paper.

8. Hydrodynamic model: results

Table 1 summarizes the results of 18 different models. Column 1 gives the shape of the crack, either parallel sides (||), narrowing at the top (Λ), widening at the top (V), or a narrowing followed by widening (X). Narrowing and widening are done with exponentials that decay with depth. The scale of the exponential in meters is given as a subscript in column 1, and the bottom-to-top widths are given as a range of values in column 2. Thus the width $\delta(z)$ in model 5 varies as $0.1 + 0.1\ e^{-z/50}$, with δ and z in meters. Similarly, the width in model 7 varies as $0.2–0.1\ e^{-z/50}$. Straight cracks have a single width from bottom to top, so only one number is given in column 2. Model 16 has $\delta(z) = 0.2 + 0.8\ e^{-z/20} – 0.6\ e^{-z/50}$, which varies from 0.2 at the bottom, to a minimum value 0.039 at $z = 40$ m, and then to 0.4 at the top.

Column 3 gives the total depth of the crack and an indication of how the heating is distributed. A single number indicates that the heat source is a reservoir below the crack. In these cases the flow enters the crack with finite velocity v_d such that $\rho_v v_d L \delta = Q$. When a range of values is given in column 3, it means that v_d is zero and the heat is distributed along the walls of the crack such that the integral of the heating is Q. The value of Q is given in column 4. Recall that 12 kW m^{-1} is close to the observed power per unit length of the tiger stripes.

Columns 5–9 are derived quantities. Column 5 gives s, the percentage of ice in the mixture as it leaves the vent. T_d is the temperature at the bottom of the crack, defined as the lowest possible temperature for which a solution exists. T_0 is the temperature at the top of the crack. V_0 is the velocity of the flow at the top of the crack – as it exits the vent. Q_{rad} is the power conducted into the ice and lost by radiation at the surface. The difference $Q - Q_{rad} \equiv Q_{vap}$ is the power carried as latent heat by the vapor as it leaves the vent.

Models 1–4 show the results of varying the width when the flow is erupting from a reservoir at the bottom of a straight crack. There is no shear heating on the walls. The heat transport mechanism is less efficient for narrower cracks, as evidenced by the rise in T_d from models 1 to 4. For these four models, T_d is the temperature of the reservoir, and it will melt if the crack width is less than 10 cm. The effects of liquid water are not included, and we do not consider models with $T_d > 273$ K. Q_{rad} goes up by a slight amount as the width decreases, because the temperatures are higher and more heat is conducted into the ice and ultimately radiated to space. Model 4 has $Q_{rad} = 6.1$ W m^{-1}, which is the largest value in the table. There are no models for which Q_{rad} approaches the observed value of 11.6 kW m^{-1}. All the models require at least two or maybe three cracks per tiger stripe to match the observed radiated power.

The values of Q_{rad} shown in Table 1 are consistent with those of Abramov and Spencer (2009), who solved for the steady-state temperature distribution in the ice with a vertical fracture held at constant temperature and a radiation-to-space condition at the surface. For a fracture temperature of 225 K, they get 3.3 GW along 520 km of tiger stripes, or $Q_{rad} = 6.3$ kW m^{-1}. The difference between this number and those in column 9 of Table 1 is small and is mostly due to our using a one-dimensional model with a parameterized form of the heat transfer. Also, they use a temperature-dependent thermal conductivity and we use a constant 3 W m^{-1} K^{-1}. Finally, we solve for the temperature profile along the fracture with a hydrodynamic model, whereas Abramov and Spencer (2009) simply impose a constant temperature as a boundary condition. The two treatments agree on the basic message—that there is a limited amount of heat that a single crack can deliver to the surface by thermal conduction, and that amount is less than the observed value. Having two or three cracks per tiger stripe would bring the models in line with the observations.

Fig. 2 shows model 1 in greater detail. The upper left panel shows the temperature, and the upper right panel shows the velocity, both as functions of the depth. The lower left panel shows s, the mass fraction of ice in the mixture, and the lower right panel shows the heat flux $F_0(z)$ into the walls due to condensation. Notice that s is positive only in the top 20 m, i.e., where $0 < z < 20$ m. As discussed earlier, the latent heat associated with negative s is included as sensible heat in Eq. (12). The most negative value of s occurs at $z = 90$ m and corresponds to a temperature difference $T - T_{wall} = -sL/C_v \approx 0.7$ K.

The heat flux rises dramatically with decreasing depth as the distance between the warm walls and the cold surface decreases. In our model the value at the surface is 110 W m^{-2}, but the actual number depends on unknown processes that are happening within 1 m of the vent. The units of $F_0(z)$ are W m^{-2}, and since there are two walls, the flux into each wall is $\frac{1}{2}F_0(z)$. This same function with x as the independent variable, $\frac{1}{2}F_0(x)$, is a fair approximation (±10%) to the power per unit area radiated from the surface as a

Table 1
Comparison of models.

1. Shape	2. Width (m)	3. d (km)	4. Q (kW m^{-1})	5. s (%) ice	6. T_d (K)	7. T_0 (K)	8. V_0 (m s^{-1})	9. Q_{rad} (kW m^{-1})
1. ||	1	4	12	0.7	236	211	320	4.9
2. ||	0.5	4	12	0.7	246	216	322	5.3
3. ||	0.2	4	12	0.7	261	222	330	5.7
4. ||	0.1	4	12	0.8	273	227	333	6.1
5. V_{50}	0.1–0.2	4	12	0.6	273	222	315	6.0
6. V_{50}	0.1–1.0	4	12	0	273	211	276	5.8
7. Λ_{50}	0.2–0.1	4	12	0.8	261	228	333	5.8
8. Λ_{20}	0.2–0.1	4	12	0.9	261	228	334	5.8
9. Λ_{20}	0.2–0.1	0.1	12	0.9	245	231	336	3.1
10. Λ_{20}	1.0–0.1	4	12	1.3	239	229	334	5.2
11. Λ_{20}	0.2–0.1	4	6	0.8	256	211	319	5.2
12. ||	0.2	4	6	0.7	256	207	316	5.1
13. ||	0.2	0–4	12	0.7	258	222	328	5.7
14. Λ_{50}	0.2–0.1	0–4	12	0.8	258	228	333	5.7
15. Λ_{50}	0.2–0.1	0–4	6	0.7	253	212	312	5.2
16. X_{40}	.2–.04–.4	0–4	12	0	262	218	261	5.9
17. || NF	0.2	0–4	12	3.1	232	221	492	3.3
18. || NF	0.1	0–4	12	2.7	238	228	453	3.0

For explanation of symbols, see Section 8.

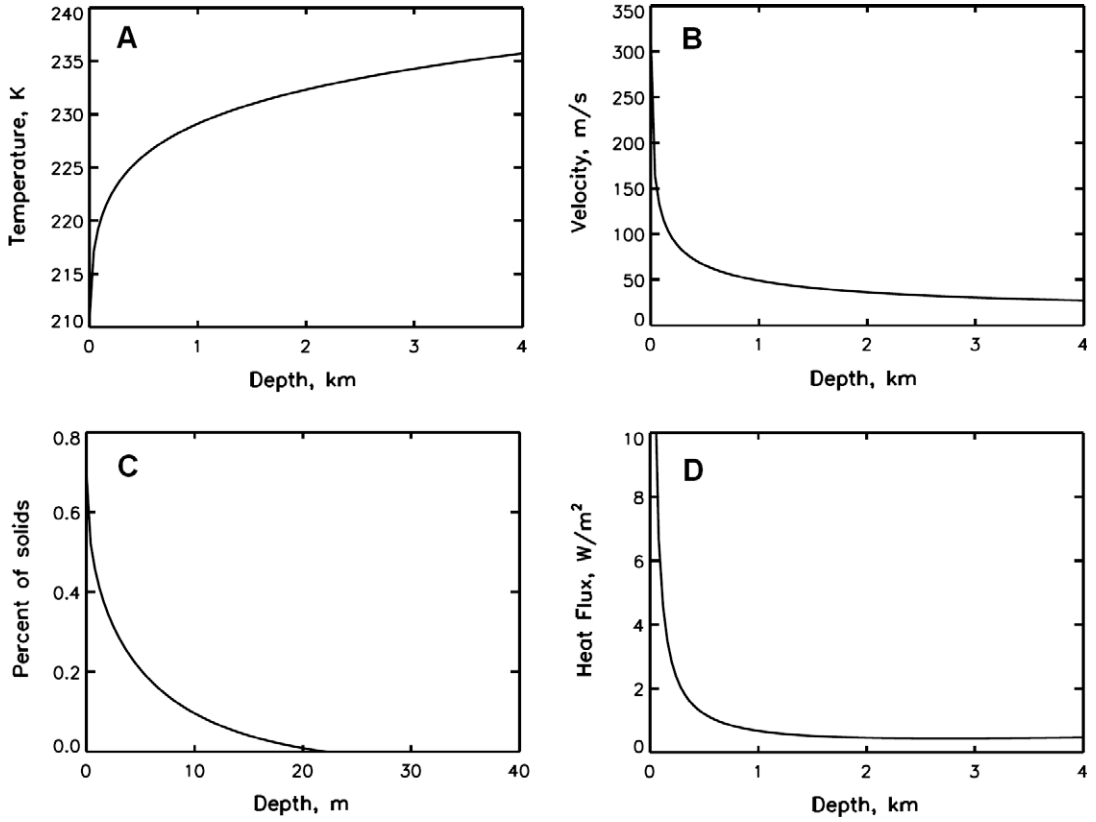

Fig. 2. Hydrodynamic model of heat transfer in a straight crack of width 1 m (model 1 in Table 1). The heat source is at the bottom of the crack, so the flow enters the crack from below carrying the heat flux $Q = 12$ kW m^{-1} as latent heat of vaporization. The temperature of the walls determines the pressure of the vapor through the SVP relation. Temperature equilibrates to a balance between evaporation, condensation, and conduction of heat to the surface. Viscous drag is included in the velocity computation. Heat flux is from the gas onto the walls as a result of condensation and release of latent heat. Solid particles do not condense in the flow. (A) Temperature. (B) Velocity. (C) Percentage of ice in the mixture. (D) Heat flux into the ice. The heat flux increases dramatically, to 110 W m^{-2} at the surface, because the temperature gradient between the warm crack and the cold surface increases as the distance between them decreases. The total radiated power $Q_{rad} = 4.9$ kW m^{-1} is less than half of the observed power, 11.6 kW m^{-1}, suggesting there are multiple cracks per tiger stripe.

function of horizontal distance x away from the crack. The integral of $\frac{1}{2}F_0(x)$ over the range $-d < x < +d$ is also a fair approximation to Q_{rad}, which is given in the last column of Table 1.

Fig. 3 shows model 6 in greater detail. This model has a 10-fold increase in the width of the crack in the last 50 m, from 0.1 m to 1.0 m. The value of s is zero, so solids cannot precipitate in this flow. Notice that $T - T_{wall}$ is never more than 2 K. Models 4 and 5 also have crack widths of 0.1 m at the deepest levels. Models 5 and 6 expand in the last 50 m, and model 4 keeps the same width at all levels, but in all three cases the temperature T_d at the bottom of the crack is 273 K. Apparently this temperature is relatively unaffected by the geometry of the crack near the surface. Similarly,

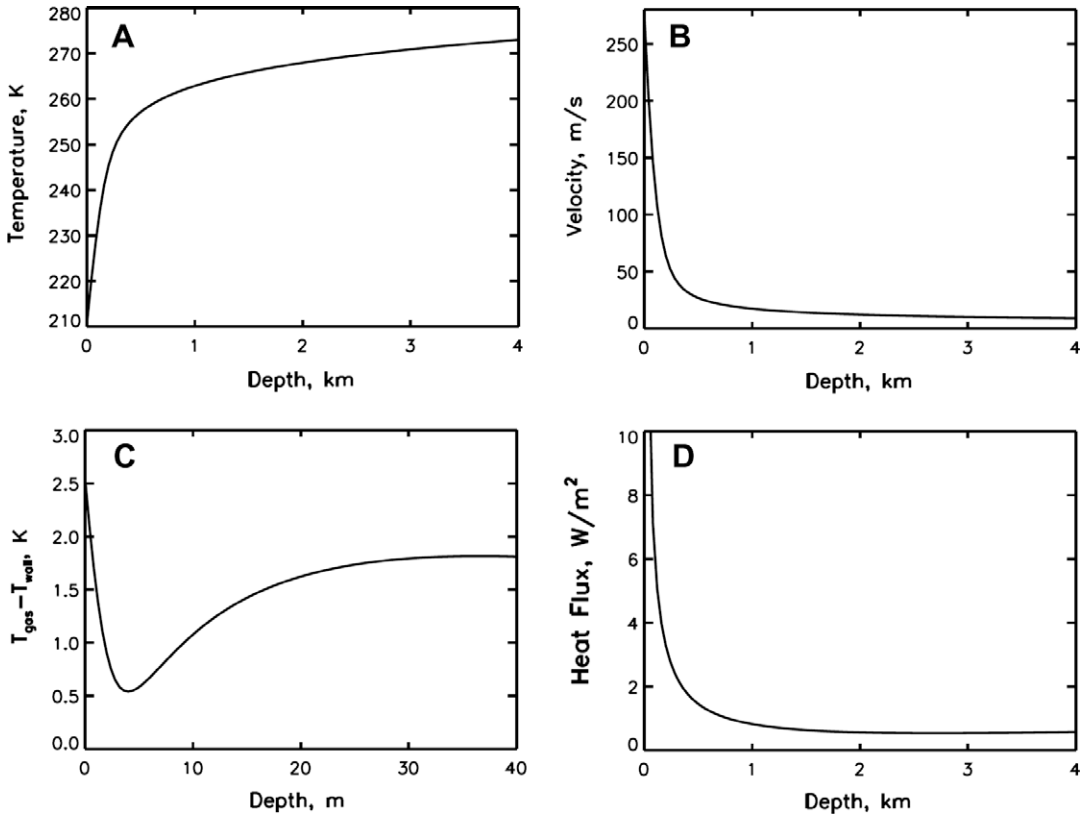

Fig. 3. Same as Fig. 2 except for a 0.1 m wide crack that expands to 1 m in the upper 50 m (model 6 of Table 1). This is one of the few cases where the gas stays warmer than the walls at all depths. As a result, no solids precipitate out of the vapor. (A) Temperature. (B) Velocity. (C) Temperature difference between gas and walls. (D) Heat flux. The total radiated power Q_{rad} is 5.8 kW m^{-1}.

models 3, 7, and 8 all have crack width = 0.2 m at depth. Models 7 and 8 have width contracting by a factor of 2; model 7 has the contraction in the top 50 m, and model 8 has it in the top 20 m. Model 3 has no contraction. Nevertheless, the value of T_d is the same, 261 K, which suggests that the width at depth is the important parameter.

Model 9 has the same width at the bottom and the same constriction at the top as model 8. Both have 12 kW m^{-1} emanating as latent heat from a reservoir at $z = d$, but the reservoir is at 100 m for model 9 and 4000 m for model 8. The temperatures at 100 m depth are almost the same: 245 K for model 9 and 243 K for model 8. The temperatures at the surface are similar as well: 231 K for model 9 and 228 for model 8. Again, the implication is that the width of the crack at depth is the important parameter.

Fig. 4 shows model 10 in greater detail. This model has the greatest contraction; the crack width goes from 1.0 m at the bottom to 0.1 m at the top over a depth range of 20 m. Temperature, velocity, and solid fraction are nearly constant until the last 10 m. The width at the bottom is the same as for model 1, and the temperature at the bottom is almost the same, 239 K vs. 236 K, respectively. The temperature at the top is greater for model 10 than for model 1. This is because the vent has to carry the same amount of vapor (and latent heat) through a narrower opening. The SVP at 229 K (model 10) is ~10 times the SVP at 211 K (model 1), which makes up for the factor of 10 difference in the width at the top.

All of the models have $Q_{rad} \leqslant 6.1$ W m^{-1}. The remainder $Q - Q_{rad}$ is Q_{vap}, the part that escapes with the vapor. For the models with $Q = 12$ kW m^{-1}, the remainder is half of the total. As mentioned at the start of Section 4, the observations imply that only ~10% of the heat is escaping with the vapor; the other 90% of the heat is conducted through the ice to the surface and ultimately lost through infrared radiation. Reducing the value of Q seems to produce models that agree more with observation. Consider the following pairs: models 8 and 11, models 3 and 12, and models 14 and 15. For each pair the geometry is the same, but the second member of the pair has $Q = 6$ kW m^{-1} and a smaller value for $1 - Q_{rad}/Q$, which is the fraction of flow carried with the vapor. There is always a critical value of Q, usually 4–5 kW m^{-1}, below which $Q_{rad} > Q$ and the flow does not reach the surface. The observations suggest that the heat flux is close to this critical value, but we do not have an explanation.

Models 13–18 have heating along the sides of the walls. The gas velocity at the bottom of the crack is zero, so there is no reservoir as there was in models 1–12. Following Nimmo et al. (2007), we assume that the heating increases linearly with depth, a result of the increasing pressure and constant shear velocity of the walls with depth. We force the heat flux to zero at the very bottom to be compatible with zero gas velocity at the bottom. Fig. 5 shows model 13 in greater detail. The geometry is the same as model 3, a straight crack of width 0.2 m and a depth of 4000 m. The heat flux into the walls $F_0(z)$ is negative at the bottom due to the heat coming out of the walls. At the top the heat conducted into the walls is greater than the local shear heating, and $F_0(z)$ is positive, as it is for models 1–12. Generally the differences between heating on the walls and heating from a reservoir are small. The temperature at depth is 258 K for model 13 and 261 K for model 3. The temperature at the surface is 222 K for both models. The same small differences occur between models 14 and 7.

Model 16 has 12 kW m^{-1} of heating on the walls and width = 0.2 m at depth. In these respects it resembles models 13 and 14, but the crack in model 16 narrows down to 0.039 m at

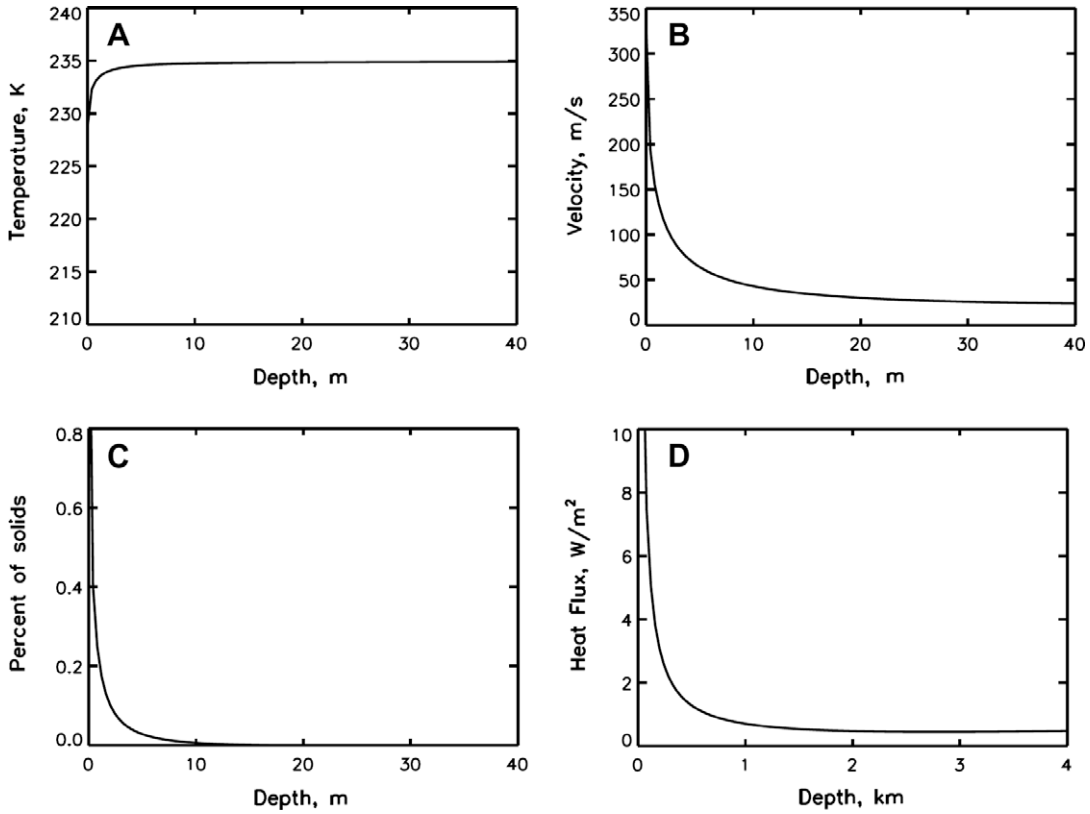

Fig. 4. Same as Fig. 2 except for a 1 m wide crack that contracts to 0.1 m in the upper 20 m (model 10 of Table 1). Temperature and velocity are nearly constant from 4 km depth up to the level where the contraction starts. Precipitation starts at ~15 m depth. (A) Temperature. (B) Velocity. (C) Percentage of ice in the mixture. (D) Heat flux. The total radiated power Q_{rad} is 5.2 kW m^{-1}.

z = 40 m before expanding to 0.4 m at the surface. Despite this constriction near the top, the temperature at depth, T_d = 262 K, is virtually the same as for models 13 and 14. It is also virtually the same as for models 3, 7, and 8, which have width = 0.2 m at depth. The temperature at the top is intermediate between models 2 and 3 because the 0.4 m width at the top, is intermediate between the widths for models 2 and 3.

Models 17 and 18 are labeled NF, which stands for no friction, and are not meant to represent reality. Compared to the more realistic models, they illustrate how important friction is in slowing down the flow and increasing the temperatures at depth. Model 17 should be compared to models 3 and 13, and model 18 should be compared to model 4. As noted in Section 7, the Reynolds number for these flows, based on the width of the channel and the mean velocity, is in the range 250–750, which is not large. Friction is important because the density of the gas is small and the kinematic viscosity $\upsilon = \eta/\rho$ is large.

Models 17 and 18 behave more like the idealized rocket nozzles in textbooks (e.g., Landau and Lifshitz, 1959). Fig. 6 shows model 17 in more detail. The transition from subsonic converging flow to supersonic diverging flow occurs at z = 580 m. Since the channel width is constant, convergence and divergence arise from the mass flux out of and into the walls, as reflected by minus the heat flux $F_0(z)$. The dashed lines show the critical subsonic solution, whose slope is discontinuous at the critical point where the velocity is equal to the speed of sound. The solid line is the smooth continuation of this solution into the supersonic regime. Since $F_0(z)/L$ is the mass flux *into* the ice, positive values represent divergent flow in the channel. Notice that $F_0(z)/L$ passes from negative to positive at the critical point. In a saturated gas the speed of sound is close to $(RT)^{1/2}$, which is 15% less than the speed of sound in unsaturated gas.

The two NF solutions have significantly higher exit velocities, larger fractions of suspended solids, and lower temperatures at the base of the crack. Model 4 has T_d = 273 K, i.e., melting at the base of the crack, but model 18 has T_d = 238 K. The higher velocities in models 17 and 18 are more in agreement with the velocities inferred from the high degree of collimation observed in stellar occultations of the plumes (Tian et al., 2007; Hansen et al., 2008). We are not suggesting that the NF models are correct. We show them first to illustrate the importance of friction, and second to help develop some intuition about the flows on Enceladus.

9. Discussion and conclusions

We addressed the questions of whether melting occurs in the icy shell of Enceladus and if it does, at what depth it occurs. To answer these questions, we developed a set of models of how the heat reaches the surface. The relevant observations are the temperatures at the surface, the total power radiated, the power carried by the gases in the plume as latent heat of vaporization, and the mass fraction of solid ice in the plume compared with ice plus vapor. We did not try to account for gases other than water vapor or compounds in the ice other than water. At least two papers have addressed this issue (Kieffer et al., 2006; Gioia et al., 2007) and have invoked hydrate clathrates to explain the roughly 10:1 ratio of water to other gases.

We have not addressed the issue of how the power is generated, although we have used the model of Nimmo et al. (2007) to provide a setting. Thus we have discussed heat generated by sliding friction in the brittle zone the upper 4–6 km and heat generated by viscous shear in the ductile zone, which starts at the base of the brittle zone and extends to the global ocean postulated by

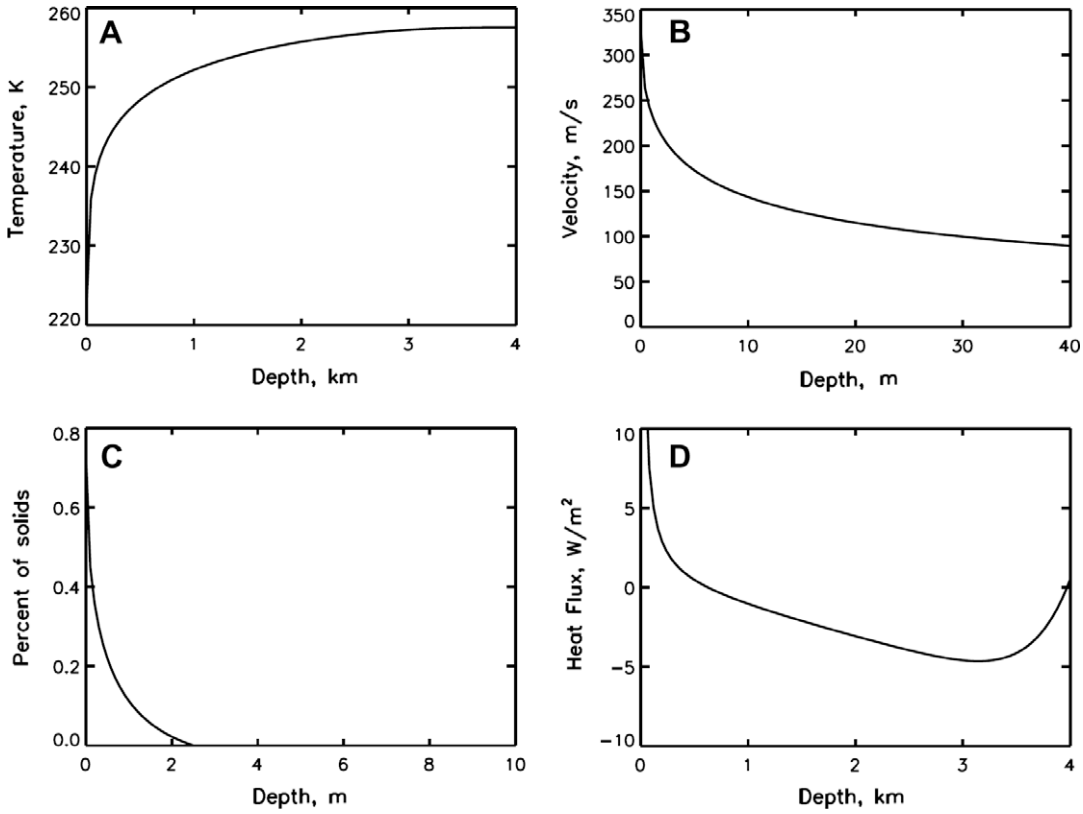

Fig. 5. Same as Fig. 2 except that all the heat is generated on the walls of the crack, so no gas enters the crack from below (model 13 of Table 1). The assumed heating profile increases linearly with depth from the surface down to a depth of 3 km, where it gradually tapers to zero at 4 km depth. The heat goes into evaporation, so the heat flux into the ice is negative at the bottom, in contrast to that in Figs. 2 and 3. The heat flux becomes positive in the upper 600 m, as the vapor condenses onto the cold ice close to the surface. Solids precipitate out of the vapor in the upper 2.5 m. (A) Temperature. (B) Velocity. (C) Percent of ice in the mixture. (D) Heat flux. Note that the zero of heat flux is in the middle of the graph. The total radiated power Q_{rad} is 5.7 kW m^{-1}.

Nimmo et al. (2007). We discussed three modes of heat transfer – thermal conduction through solid ice, vapor diffusion through an icy matrix, and flow of liquid and vapor through an open crack. We note an important principle—that the partial pressure of the vapor is always the same as the saturation vapor pressure of the icy walls of the crack.

There are no easy answers to the questions we set out to answer. The source regions can get rid of their heat without melting if they have efficient modes of transferring heat to the surface. For diffusion through a porous regolith, melting does not occur if the grains are larger than ~1 cm and the porosity is larger than 0.1. For hydrodynamic flow in open cracks, melting does not occur if the heat is generated on the crack and the width is greater than ~10 cm. Further, melting is less likely if there are several cracks per tiger stripe. Since the width, depth, and number of cracks are still unknown, we are skeptical of theoretical arguments that are strongly for (e.g., Schmidt et al., 2008; Hansen et al., 2008) or strongly against (Gioia et al., 2007; Nimmo et al., 2007) temperatures above 0 °C in the upper 5 or 10 km of the ice. The best evidence probably comes from observations of particle composition (Postberg et al., 2008), which support the hypothesis of a dynamic interaction of Enceladus' rocky core with liquid water.

Hydrodynamic flow in open cracks that are wider than ~10 cm provides an efficient mode of heat transfer, but the source of the heat must be close to the crack. The source will warm up if it is separated from the crack by distances of km, because then the heat has to diffuse through the ice before it can be carried by the flow to the surface. This is the difference between the brittle zone and the ductile zone in the Nimmo et al. (2007) model. The former has cracks and the latter does not, so the heat generated in the ductile zone has to diffuse through the ice over distances of several km. Such diffusion could lead to melting.

To the best of our knowledge, no one has tried to calculate the width or depth of the cracks from first principles. The crack dimensions are controlled not only by the tidal stresses but also by evaporation and condensation. This is a shortcoming of current work, including our own. No one has solved the time-dependent thermal problem as a crack opens up and a plume develops, ending perhaps when the crack seals itself off. The flow in the crack is extremely sensitive to the wall temperature, which depends on the thermal history. The time for the plume to reach the surface in cold ice depends on the heat flux, and is roughly the same whether the fluid in the crack is liquid water or water vapor. We estimate this time as ~67 years. The time for the crack to seal itself off by condensation in the upper few meters is ~1 year, and this poses a problem: The lifetime of a crack is less than the time to create it. Cracks may wander around at the surface on scales of meters and times of years, but such wandering is below the current detection limit. Neglect of such transient behavior is a major limitation of the present work.

Speeds are another problem. As shown in Table 1, our models do not give speeds above 340 m s^{-1}, which is faster than the 235 m s^{-1} escape velocity from Enceladus but slower than the velocities inferred from the collimation of the plumes (Tian et al., 2007; Hansen et al., 2008). The latter is an indirect inference: The gas in the plumes is assumed to spread laterally at the thermal speed of the molecules. That speed divided by the tangent of the observed spreading angle is the vertical speed, which is inferred to be ~600 m s^{-1}. Viscous drag with the walls slows the flow in our model to speeds that are much less than the theoretical maximum speed, $(2C_pT)^{1/2} \approx 900$ m s^{-1}. If the cracks are not straight,

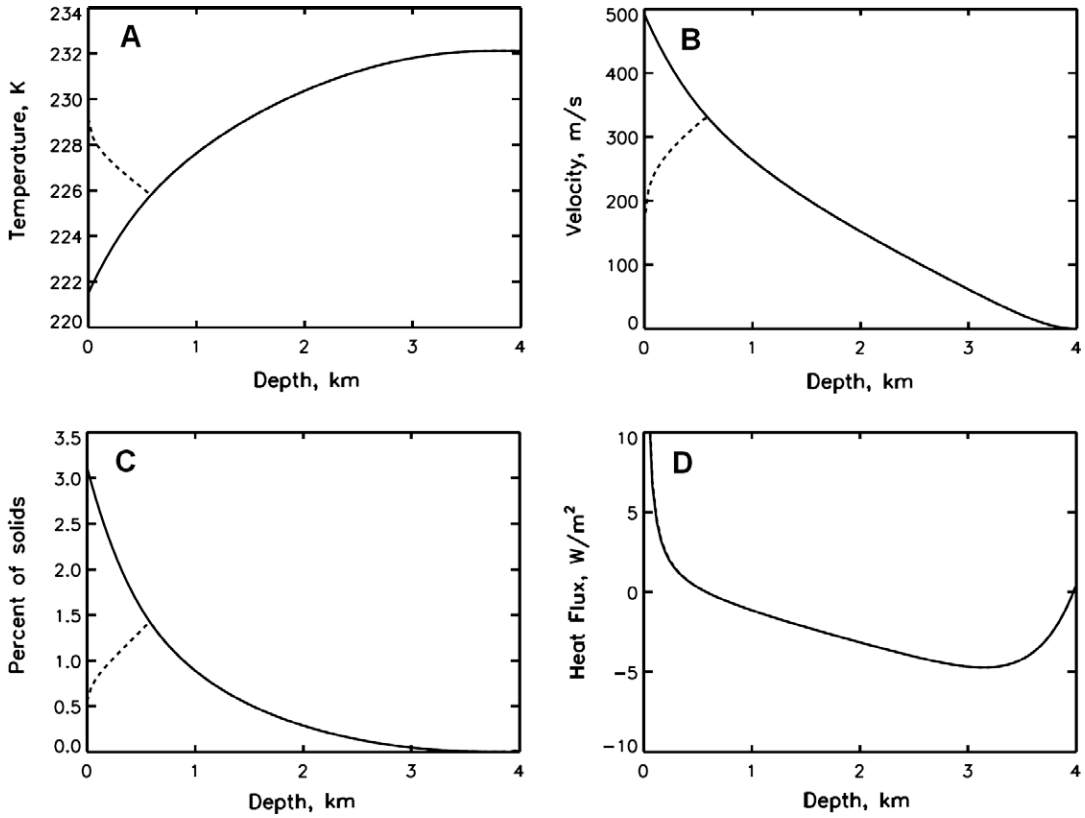

Fig. 6. Same as Fig. 2 except that friction with the walls has been artificially suppressed (model 17 of Table 1). As in Fig. 5, all the heat is generated on the walls, so the heat flux into the wall is negative at the bottom and positive at the top. Without friction the flow becomes supersonic before reaching the surface. The transition occurs at a depth of 580 m, which is also the depth at which the heat flux changes sign. The solid line is the supersonic solution and the dashed line is the subsonic solution. Compared to models with friction, this model is colder, has higher velocity, and has a higher percentage of ice in the mixture. (A) Temperature. (B) Velocity. (C) Percent of ice in the mixture. (D) Heat flux. Note that the zero of heat flux is in the middle of the graph. The total radiated power Q_{rad} is 3.3 kW m^{-1}.

collisions with the walls could slow the particles further (Schmidt et al., 2008).

In models 1–16 the largest value of s, the mass fraction of solid ice, is only 1.3%. Porco et al. (2006), on the other hand, used Cassini UVIS and ISS observations to infer that the mass of ice is comparable to the mass of vapor. They claim that the large ice/gas ratio argues against ice condensing out of the vapor, as would be expected for the subliming ice model. Our results are consistent with this claim, but we are not ready to reject the subliming ice model—the model of Table 1—and conclude that the plumes arise from a boiling liquid. For one thing, our model assumes steady state. We have not considered the history of the cracks or the transient nature of the temperature distribution on the walls of the crack. Moreover, the Porco et al. estimate could be too large, as pointed out by Kieffer et al. (2009), since the conversion of brightness in the ISS images into mass of the particles is dependent on particle size, which is not well known. Hedman et al. (2009) estimate that the particle mass flux is between 2 and 200 kg s^{-1}, which may be comparable to the total mass flux in the gas, in agreement with the Porco et al. (2006) result. These problems can be solved, but their solution is beyond the scope of this paper.

Particle properties hold important clues to subsurface conditions, but we have not pursued that topic here. Schmidt et al. (2008) have a model for particles condensing directly out of the vapor. Their model includes homogeneous nucleation and collisions of the particles with the walls, but it does not include viscous drag or mass flux going into or out of the walls. The temperature of the walls does not enter in their calculations. We have shown that the temperature of the walls is important, because the partial pressure of the vapor in the crack is essentially equal to the SVP of the walls.

We briefly considered cracks filled with liquid water. The hydrostatic pressure of the liquid tends to hold the crack open against mechanical stresses. This is an advantage that the liquid has. A disadvantage is that the latent heat of fusion is seven times less than the latent heat of vaporization, so the liquid has to condense at a greater rate to keep the walls of the crack warm. In other words, the crack tends to seal itself off faster when it is filled with liquid than when it is filled with vapor. Further, the liquid cannot reach the surface by hydrostatic pressure only. Whether the liquid will boil when exposed to vacuum at 0 °C depends on nucleation in the liquid, which is another open question.

Acknowledgments

This research was supported by a Grant from the Director's Research and Development Fund of the Jet Propulsion Laboratory (Task number 07DO1236) and by a Grant from the Astronomy and Astrophysics Research Grants Program of the National Science Foundation (Award number AST-0808148). We thank Francis Nimmo, Jürgen Schmidt, and John Spencer for useful discussions. The research was performed at the California Institute of Technology, Pasadena, CA 91125, USA.

References

Abramov, O., Spencer, J.R., 2009. Endogenic heat from Enceladus' south polar fractures: New observations, and models of conductive surface heating. Icarus 199, 189–196. doi:10.1016/j.icarus.2008.07.016.

Arya, S.P., 1988. Introduction to Micrometeorology, second ed. Academic Press, San Diego, pp. 152–153.

Brilliantov, N.V., Schmidt, J., Spahn, F., 2008. Geysers of Enceladus: Quantitative analysis of qualitative models. Planet. Space Sci. 56, 1596–1606.
Clifford, S.M., Hillel, D., 1983. The stability of ground ice in the equatorial region of Mars. J. Geophys. Res. 88, 2456–2474.
Crawford, G.D., Stevenson, D.J., 1988. Gas-driven water volcanism and the resurfacing of Europa. Icarus 73, 66–79.
Crifo, J.F., 1989. Inferences concerning water vapor viscosity and mean free path at low temperatures. Astron. Astrophys. 223, 365–368.
Gaidos, E.J., Nimmo, F., 2000. Planetary science – Tectonics and water on Europa. Nature 405. 637–637.
Gioia, G., Chakraborty, P., Marshak, S., Kieffer, S.W., 2007. Unified model of tectonics and heat transport in a frigid Enceladus. Pub. Nat. Acad. Sci. 104, 13578–13581.
Goldsby, D.L., Kohlstadt, D.L., 2001. Superplastic deformation of ice: Experimental observations. J. Geophys. Res. 106, 11017–11030.
Hansen, C.J., Esposito, L.W., Stewart, A.I.F., Colwell, J., Hendrix, A., Pryor, W., Shemansky, D., West, R., 2006. Enceladus' water vapor plume. Science 311, 1422–1425.
Hansen, C.J., Esposito, L.W., Stewart, A.I.F., Meinke, B., Wallis, B., Colwell, J.E., Hendrix, A.R., Larsen, K., Pryor, W., Tian, F., 2008. Water vapor jets inside the plume of gas leaving Enceladus. Nature 456, 477–479.
Hedman, M.M., Nicholsen, P.D., Showalter, M.R., Brown, R.H., Buratti, B.J., Clark, R.N., 2009. Spectral observations of the Enceladus plume with Cassini-VIMS. Astrophys. J. 693, 1749–1762.
Hurford, T.A., Helfenstein, P., Hoppa, G.V., Greenberg, R., Bills, B.G., 2007. Eruptions arising from tidally controlled periodic openings of rifts on Enceladus. Nature 447, 292–294.
Jeans, J.H., 1954. The Dynamical Theory of Gases, fourth ed. Dover Publications, New York, pp. 121–122.
Kieffer, S.W., Lu, X., Bethke, C.M., Spencer, J.R., Marshak, S., Navrotsky, A., 2006. A clathrate reservoir hypothesis for Enceladus' south polar plume. Science 314, 1764–1766.
Kieffer, S.W., Lu, X., McFarquar, G., Wohletz, K.H., 2009. A redetermination of the ice/vapor ratio of Enceladus' plumes: Implications for sublimation and the lack of a liquid water reservoir. Icarus 203, 238–241. doi:10.1016/j.icarus.2009.05.011.
Landau, L.D., Lifshitz, E.M., 1959. Fluid Mechanics. Pergamon Press, London, pp. 313–317 and 347–350.
Lide, D.R. (Ed.), 1993. Handbook of Chemistry and Physics, 74th ed. CRC Press, Boca Raton, Florida, pp. 6–14.
Mitri, G., Showman, A., 2005. Convective–conductive transitions and sensitivity of a convecting ice shell to perturbations in heat flux and tidal-heating rate: Implications for Europa. Icarus 177, 447–460. doi:10.1016/j.icarus.2005.03.019.
Nimmo, F., Gaidos, E., 2002. Strike-slip motion and double ridge formation on Europa. J. Geophys. Res. 107 (E4). doi:10.1029/2000JE001476.
Nimmo, F., Spencer, J.R., Pappalardo, R.T., Mullen, M.E., 2007. Shear heating as the origin of the plumes and heat flux on Enceladus. Nature 447, 289–291.
Porco, C.C., and 24 colleagues, 2006. Cassini observes the active south pole of Enceladus. Science 311, 1393–1401.
Postberg, F., Kempf, S., Hillier, J.K., Srama, R., Green, S.F., McBride, N., Grün, E., 2008. The E-ring in the vicinity of Enceladus II. Probing the moon's interior—The composition of E-ring particles. Icarus 193, 438–454.
Schmidt, J., Brilliantov, N., Spahn, F., Kempf, S., 2008. Slow dust in Enceladus' plume from condensation and wall collisions in tiger stripe fractures. Nature 451, 685–688.
Spencer, J.R., Pearl, J.C., Segura, M., Flasar, F.M., Mamoutkine, A., Romani, P., Buratti, B.J., Hendrix, A.R., Spilker, L.J., Lopes, R.M.C., 2006. Cassini encounters Enceladus: Background and the discovery of a south polar hot spot. Science 311, 1401–1405.
Spitale, J.N., Porco, C.C., 2007. Association of the jets of Enceladus with the warmest regions on its south-polar fractures. Nature 449, 695–697.
Tian, F., Stewart, A.E.F., Toon, O.B., Larsen, K.W., Esposito, L.W., 2007. Monte Carlo simulations of the water vapor plumes on Enceladus. Icarus 188, 154–161.
Turcotte, D.L., Schubert, G., 2002. Geodynamics, second ed. Cambridge University Press, Cambridge, UK, pp. 375–376.
Waite, J.H., and 14 colleagues, 2006. Cassini ion and neutral mass spectrometer: Enceladus plume composition and structure. Science 311, 1419–1422.